Eur Respir J 2001; 18: 381–392
Printed in UK – all rights reserved

European Respiratory Journal
ISSN 0903-1936

SERIES "THORACIC IMAGING"
Edited by P.A. Gevenois, A. Bankier and Y. Sibille
Number 6 in this Series

Virtual tools for imaging of the thorax

G.R. Ferretti, I. Bricault, M. Coulomb

Virtual tools for imaging of the thorax. G.R. Ferretti, I. Bricault, M. Coulomb. ©ERS Journals Ltd 2001.

ABSTRACT: Helical computed tomography (HCT) allows for volume acquisition of the entire thorax during a single apnoea. Combination of HCT acquisition with synchronous vascular enhancement gives rise to HCT angiography (HCTA).

In the last decade, HCT and HCTA have revolutionized the diagnosis of thoracic diseases, modifying many diagnostic algorithms. Because HCT provides for a true volume acquisition free of respiratory misregistration, three-dimensional (3D) rendering techniques can be applied to HCT acquisitions.

As these 3D rendering techniques present the HCT information in a different format to the conventional transaxial CT slices, they can be summarized as virtual tools.

The purpose of this review is to give the readers the most important technical aspects of virtual tools, to report their application to the thorax, to answer clinical and scientific questions, and to stress their importance for patient management, clinical decision making, and research.

Eur Respir J 2001; 18: 381–392.

Dept of Radiology, Hôpital Michallon, Centre Hospitalier Universitaire, Grenoble Cedex 09, France.

Correspondence: G.R. Ferretti, Service Central de Radiologie et Imagerie Médicale, Centre Hospitalier Universitaire, Grenoble BP 217, F-38043 Grenoble cedex 09, France.
Fax: 33 476765901

Keywords: Computed tomography
helical computed tomography
maximum intensity projection
minimum intensity projection
virtual rendering
volume rendering

Received: October 10 2000
Accepted after revision February 21 2001

Volume acquisition of the thorax during one breath-hold is possible using helical computed tomography (HCT) [1]. HCT of the thorax has become a major noninvasive technique for the evaluation of the airways, the mediastinum, the major thoracic vessels, the chest wall, and, in some instances, the pulmonary parenchyma [2–4]. It has replaced conventional or slice-by-slice computed tomography (CT) acquisition, except for high resolution computed tomography (HRCT) of the pulmonary parenchyma. Because HCT provides a thorough volumetric acquisition of the thorax, HCT acquisitions can be reconstructed as contiguous or overlapped transaxial CT images (the conventional way to display CT images) or as three-dimensional (3D) images by using various 3D software [5–7]. 3D reconstructions are now widely available and have gained popularity among radiologists who use them to answer specific clinical problems [8]. Although 3D images contain no more information than the axial CT images, they provide information in other formats that can enhance the perception of the anatomy. These reconstructions include multiplanar reformation (MPR), maximum intensity projection (MIP) and minimum intensity projection (IP_{min}), three-dimensional surface shaded display (3D SSD), and volume rendering (VR).

The purpose of this review is to give the readers the most important technical aspects of 3D virtual images, their strengths and weaknesses, to report their application to clinical and scientific questions, and to stress their importance for patient management, clinical decision making, and research.

Technical aspects

HCT acquisition is a major technical evolution of CT that was introduced in the early 1990s [1]. It combines the continuous rotation of the X-ray tube with the advancement at a constant speed of the patient through the gantry during the emission of X-rays. Therefore, the X-ray beam describes a helical

Previous articles in this series: No. 1: Ghaye B, Dondelinger RF. Imaging guided thoracic interventions. *Eur Respir J* 2001; 17: 507–528. **No. 2:** Vansteenkiste JF, Stroobants SG. The role of positron emission tomography with ^{18}F-fluoro-2-deoxy-D-glucose in respiratory oncology. *Eur Respir J* 2001; 17: 802–820. **No. 3:** Kauczor HU, Chen XJ, van Beek EJR, Schreiber WG. Pulmonary ventilation imaged by magnetic resonance: at the doorstep of clinical application. *Eur Respir J* 2001; 17: 1008–1023. **No. 4:** Hansell DM. Small airways diseases: detection and insights with computed tomography. *Eur Respir J* 2001; 17: 1294–1313. **No. 5:** Franquet T. Imaging of pneumonia: trends and algorithms. *Eur Respir J* 2001; 18: 196–208.

course around the patient and gives rise to a volume of data.

Helical computed tomography protocols

Whatever software is used, generating 3D images requires three main steps: data acquisition, data processing, and data display.

Data acquisition

The choice of HCT parameters is of paramount importance in generating accurate visualization of the thoracic anatomy. Using different scanner models, many reports [9, 10] have emphasized the importance of selecting the thinnest collimation, pitch value (ratio of the table increment per rotation and slice collimation) around 1, and to reconstruct axial slices with an overlap of $\geqslant$30%. In clinical practice, the radiologist has to find a compromise between the slice thickness and the pitch value compatible with the acquisition of the thoracic volume of interest during a single breath-hold. Of these parameters, slice thickness has the greatest impact on the quality of 3D-reconstructions [10]. Therefore, using state of the art single detector HCT scanners with subsecond rotation time (0.75 or 0.8 s), an acceptable compromise is reached using 2-mm or 3-mm collimation, a pitch value ranging from 1.5–2.30% to 50% overlap index, and a low spatial resolution algorithm. In some cases, a HCT scanner using thinner collimation (1 mm) is required to analyse the lung parenchyma or the subsegmental bronchi. Introduction of the multiple detector-row technology [11] permits the performance of faster acquisitions for a given volume while using thinner collimation, thereby increasing the overall quality of 3D simulations. Using this new technology, it is now possible to acquire the entire thorax during one apnoea with 1-mm slice sections.

Contrast media administration is usually needed to analyse the vessels of the thorax and gives rise to HCT angiography. A review of the protocols of contrast media administration is beyond the scope of this paper and can be found in a recent state of the art study [4]. Analysis of the airways does not require intravascular contrast injection, because of the great natural contrast between the airways and their environment.

Radiation dose to the patients is a great concern and should be minimized at the lowest level possible without making compromises in image quality. Because of the great natural contrast (air-tissue interfaces) of the thorax, low kilovoltage (100–120 kV) and milliamperage (100–150 mA) can be used. HCT offers the opportunity to reduce the radiation dose as compared to slice-by-slice contiguous acquisition while acquiring the entire volume of data, if a pitch value >1 is selected.

Once acquired, CT images are transferred *via* a local network to a 3D workstation where they are processed.

Image processing

Virtual tools can be divided into techniques that create planar images such MPR and techniques that produce 3D images.

Multiplanar reformation. MPR is the most popular tool in clinical practice [7]. It consists of creating images of 1 voxel thick in any arbitrary plane of the volume of acquisition. MPRs eliminate superimposition of voxels lying outside the selected plane. Planar or curvilinear MPR can be interactively and instantaneously created along a structure of interest. Images are displayed in the conventional Hounsfield's scale, which precludes the loss of information due to segmentation.

Three-dimensional reconstructions. 3D reconstruction software uses three main algorithms: maximum and minimum intensity projection, surface rendering, and VR.

Maximum intensity projection and minimum intensity projection. MIP and IPmin are based on the same principal: imaginary rays are projected through a subvolume of original data set [12]. The rays are parallel (orthogonal projection) and select some specific voxels along their route inside the volume. MIP algorithm selects the voxel with the highest attenuation along each ray, while IPmin algorithm selects the voxel with the lowest attenuation along the rays. This process is instantaneous. The final image is, therefore, a projection of the highest or lowest attenuation voxels of the initial volume with no depth information. MIP has been the most popular method of obtaining CT angiographic images [13].

MIP and IPmin algorithms have been applied to high-resolution (1 mm) volume acquisition of a selected volume of lung parenchyma without contrast media injection [14–16]. This technique is called sliding thin slab (STS), or multiplanar volume reconstruction (MPVR), MIP or IPmin. The main value of both STS MIP and STS IPmin is that they extract specific information based on density value within the volume. The main drawbacks of MIP, STS, MIP, and STS IPmin are the absence of depth information, the superimposition of complex anatomic structures, and the loss of density information [14].

Three-dimensional surface shaded display. 3D SSD is the most frequently used algorithm to create 3D views of the central airways, the pulmonary vessels, and the thoracic wall. The goal of the 3D SSD algorithms is to isolate the surface of an anatomical structure of interest from the initial volume of data. The voxels constituting the structure to display are isolated from the surrounding voxels based on their density properties using threshold segmentation [5]. Manual segmentation is often used. Segmentation results in a binary classification of the voxels constituting the volume of data: voxels within the threshold values are retained for rendering and voxels out of the threshold values are removed. The information loss is therefore remarkable. The impression of depth and relief is given in illuminating the isolated surface with an imaginary source of light.

Volume rendering

This is a sophisticated true volumetric rendering technique in which the different tissues of interest are encoded with varying opacity and colour. Voxels are displayed according to the percentage of a given tissue of interest included in each voxel. All voxels of the initial data set are preserved in their original anatomical spatial relationships [5, 17].

Both surface and volume rendering can be used to either create external models of the anatomy or internal simulations.

External rendering. 3D SSD provides external views of anatomical relationships of complex structures that have high contrast such as bones, contrast enhanced vessels, or the tracheobronchial tree. The main limitation of this technique is that the selected surface is highly dependent on the choice of an arbitrary threshold level. As a result, the size of a structure can be artificially reduced or increased depending on the chosen threshold. Therefore, 3D SSD models must be displayed with axial or MPR images to select adapted threshold values. This tool can be time consuming (15–30 min) in the case of complex anatomy.

VR has been introduced more recently. It requires more computer power and time editing than 3D SSD. It offers the opportunity to create semitransparent tissue planes enhancing the perception of the anatomy. At the level of central airways, VR allows creation of virtual bronchography images that are very similar to conventional bronchograms [18].

Internal rendering. Virtual endoscopy (VE) is one of the most recently developed 3D techniques that is applicable to the tracheobronchial tree [19, 20] or the pulmonary artery [21]. VE simulates an endoscopist's view of the internal surface of the airways or the vessels thanks to perspective rendering algorithm, with no invasiveness. Both surface [19, 20] and VR [6] are used.

VE with surface shaded display requires defining threshold values in order to isolate voxels that are presumed to represent the inner wall of the structures. The isolated structures are then displayed using artificial grey scale based on their orientation and position relative to the tip of the virtual camera. The results of SSD VE simulations are highly dependent on the choice of threshold values. Therefore, surface discontinuities, artificial narrowing and floating pixels may be present. SSD VE is also very sensitive to partial volume effects. Careful review of VE images along with axial CT or MPR images allows the selection of optimal threshold values and minimizes artefacts and pitfalls. The navigation through the airways is performed manually with the computer mouse or computed automatically [22]. During the progression of the virtual endoscope, the position of the camera is tracked on MPRs or 3D SSD that are simultaneously displayed along with VE. The angle of orientation and aperture (30–120°) of the virtual camera is adaptable in real time. SSD VE requires less computer power and proceeds more rapidly than VR VE [4].

VR has been used to create VE. VR VE permits visualization of peribronchial structures through bronchial or vessels walls and is less sensitive to partial volume effects than surface rendering [4].

Powerful computers reconstruct VE simulations at a speed that permits real time rendering (15–25 images·s^{-1}) and, therefore, "flying" within the airways in a virtual manner is possible [19]. With conventional data workstations, screening of the proximal airways requires between 15–45 min.

VE is applicable to the major airways up to a segmental level using 2- or 3-mm slice thickness and to subsegmental bronchi using 1-mm sections.

Virtual angioscopy has been applied to major vessels (pulmonary artery, aorta, superior vena cava (SVC)) [21]. It uses the same software as virtual bronchoscopy but requires the selection of adapted threshold values to visualize the internal surface of contrast enhanced vessels.

Display

3D images are created on dedicated workstations. Images are then available on the computer screen for interactive display. They can be filmed on hard copy films, recorded on video, or sent through the internet to a distant computer.

Clinical applications

Although virtual tools can be applied to any anatomical compartment of the thorax, clinical experience has shown that some tools are of greater interest in some anatomical structures than in others.

Central airways

HCT has improved CT imaging of the central airways by providing continuous thin sections of the airways free of respiratory artefacts [23, 24]. However, axial CT images are perpendicular or oblique to the main axis of the trachea and bronchi, which creates difficulties in detecting and depicting abnormalities. Virtual tools offer the opportunity to visualize the trachea and bronchi along their main axis, on external 3D views or on internal bronchoscopic images.

MPRs are of particular value for the evaluation of focal airway stenoses (fig. 1). In a series including 27 patients, following lung transplantation, QUINT *et al.* [25] showed that MPRs were 94% sensitive in detecting focal airway stenoses as compared to 91% for axial CT images. MPRs allowed an easier and accurate evaluation of mild stenoses, extent of the stenoses, and bronchial dehiscence. MACADAMS *et al.* [26] confirmed the usefulness of MPRs through the assessment of bronchial anastomoses following lung

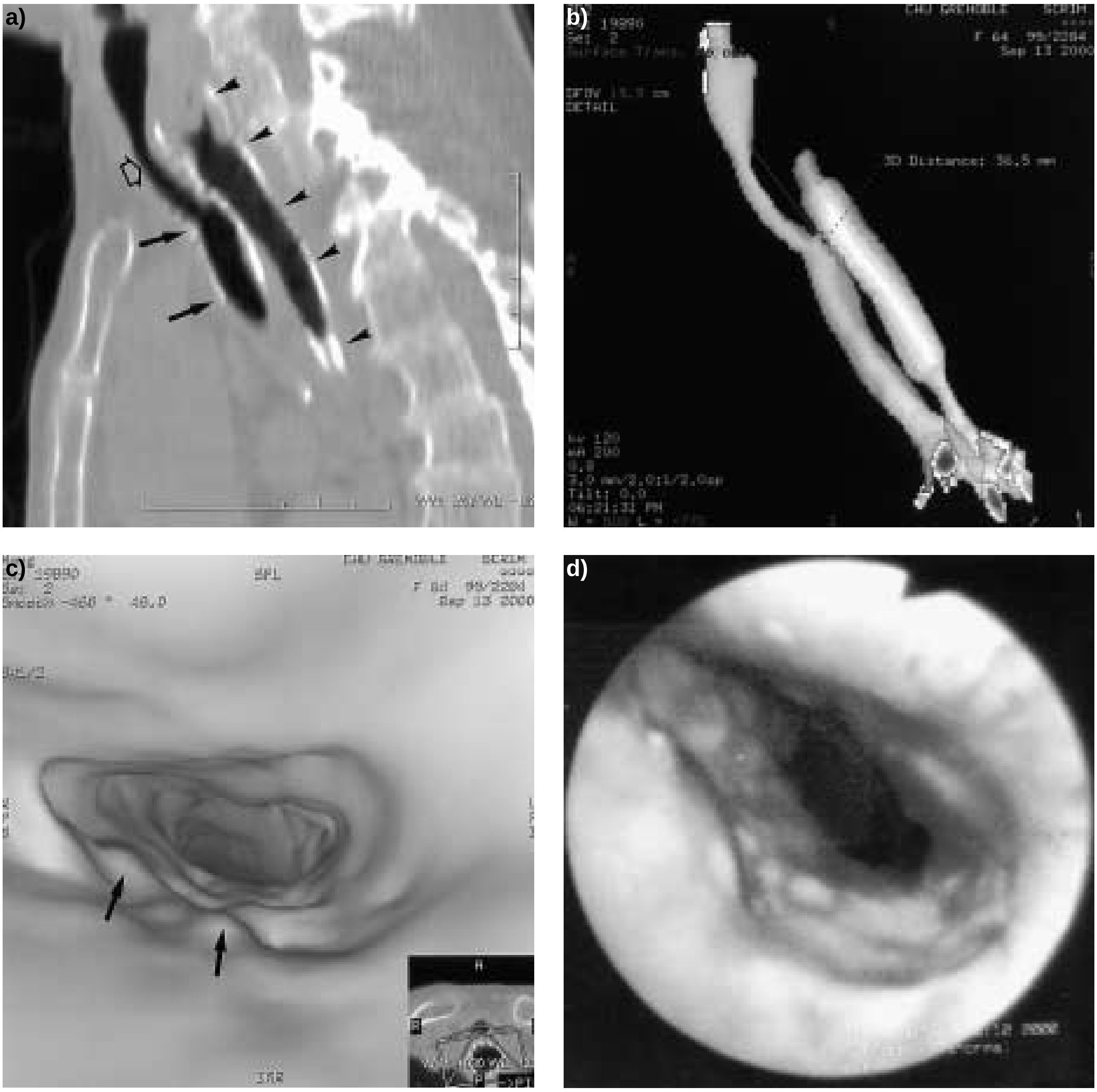

Fig. 1. – A 64-yr-old female with history of tracheal tumour. A stent was inserted in the trachea 3 yrs ago. The patient complains of recurrent dyspnoea 3 months after insertion of a stent in the oesophagus because of severe dysphagia. a) Sagittal multiplanar reformation shows the stent in the trachea (arrows), the stent in the oesophagus (arrowheads), and a stenosis of the trachea above the stent (empty arrow), which is due to extrinsic compression by the stent inserted in the oesophagus. b) Three-dimensional surface shaded display in a lateral projection allows for precise measurement of the length of the tracheal stenosis before stenting. c) Virtual endoscopy shows the tracheal stenosis and the prints of the stent (arrows). d) Fibreoptic bronchoscopy at the same level as 1c.

transplant. In a series including 64 patients with stenoses of the central airway, MPR was found to be as accurate (99%) as axial CT images in the detection of obstructive airway lesions, detected using fibreoptic bronchoscopy (FOB) [27], and was more accurate than 3D SSD (90%) and IP_{min} (81%). Concerning the characterization of the stenoses (*i.e.* severity, length, and shape), axial CT images, MPR, 3D SSD, and IP_{min} were not statistically different. The resectability of bronchogenic carcinoma and hilar and mediastinal structures can be assessed by HCT with MPRs of the airways and the pulmonary vessels [28]. MPRs were found to provide a better understanding of tumour implantation as compared to cross-sectional images and endoscopic examination [29]. Finally, MPRs are useful in understanding congenital airway diseases [30].

STS MIP is not indicated as detecting central airway stenoses because it selects the highest attenuation voxels, which artificially increases the size of stenoses in eliminating air-containing voxels. In contrast, STS IP_{min} artificially decreases the size of asymmetrical stenoses by specifically selecting air-containing voxels [27].

External 3D SSD images allow for a better understanding of the longitudinal extent of airway stenoses than axial CT images [31]. These images offer an overview of the pathology and have been found useful in complex airway anatomy, including congenital airway diseases, and in identifying extraluminal air (*i.e.* tracheobronchial diverticuli, fistulae, and air leaks, bronchial distortion following surgery). RÉMY-JARDIN *et al.* [19] evaluated external VR (virtual bronchography) images in comparison with axial CT images in a series of 74 patients known or suspected of abnormalities of the airways (benign stenoses: 47; complex airway lesions: 15; bronchiectasis: 12). These authors concluded that VR added diagnostic or morphological information in 31% of patients, improved confidence in the interpretation of congenital airway diseases in 8%, and corrected interpretative errors in 5% of cases. VR was of particular interest in diagnosing mild changes in airway calibre and understanding complex tracheobronchial abnormalities [18].

Internal simulations of the airways (*e.g.* virtual bronchoscopy (VB)) produce remarkably high-quality and accurate reproductions of major endoluminal abnormalities (fig. 2) [19, 32, 33]. VB has some advantages over real bronchoscopy: it is noninvasive, recurrent views can be created, and directions of view of the virtual endoscope may be changed interactively. However, in comparison to FOB, VB has many limitations: it does not show the mucosa, its colour, vascularity, oedema, friability or the dynamic of the bronchi, and does not provide for biopsy or bacteriological samples [34]. Many potential clinical applications of VB have been proposed [34], such as screening airways for endobronchial tumours, characterizing endobronchial abnormalities, guiding transbronchial needle aspiration, guiding interventional bronchoscopy, and assessing tracheobronchial stenoses.

Regarding the detection of endobronchial tumours, VB is limited to the demonstration of tumours that modify the calibre of the airways. All space occupying tumours >5 mm in diameter were demonstrated using SSD VB [32]. However, mild stenoses, submucosal infiltration, and superficial spreading tumours are not identified [32,33]. Furthermore, VB is unable to identify the causes of bronchial obstruction (*i.e.* bronchogenic carcinoma, benign tumour, mucus plugging, blood clot, or foreign body) [33, 35]. Many series have shown the excellent correlation between VB images and FOB results regarding the location, severity, and shape of airway narrowing [19, 32, 36]. VB is able to pass severe airway stenoses or obstructions, which is not possible using FOB. Automatic detection of polypoid lesions of the airways has been proposed by SUMMERS *et al.* [37], but the sensitivity of the technique has to be improved. The added diagnostic value of VB in patients known to have benign abnormalities and carcinoid tumours of the airways [38] has been studied in a series of 28 patients with 32 abnormalities. The sensitivity for detection of abnormal bronchial segments was 89% using axial CT images, and 92% using axial CT images with VB. Specificity reached 99% in both cases. Regarding the potential role of VB in characterizing benign endobronchial lesions, VB added little information to axial CT images [38], as the correct diagnosis of the nature of bronchial abnormalities increased from 68% with axial CT images to 76% when VB where interpreted together with axial CT images. However, display of VB images increases the confidence of pulmonologists in CT results [38].

VB with VR has been proposed to guide transbronchial needle aspiration (TBNA) [39]. Simultaneous display of the real endoscopic views and the virtual views, showing the inner wall of the airway and the nodes to biopsy as well as the vessels to avoid, increased the confidence of bronchoscopists, shortened the preparation time of TBNA, and shortened the time of the procedure [39]. In a preliminary study that included 17 patients with mediastinal adenopathy, the sensitivity of TBNA reached 88% on a per node basis analysis. These encouraging results should be confirmed in a larger series involving bronchoscopists on a learning curve [34]. Computer-assisted transbronchial biopsy system was described [40]. The aim of the software is to match VB images showing the target to sample with FOB in real time. HCT is acquired before FOB. VB simulations showing the

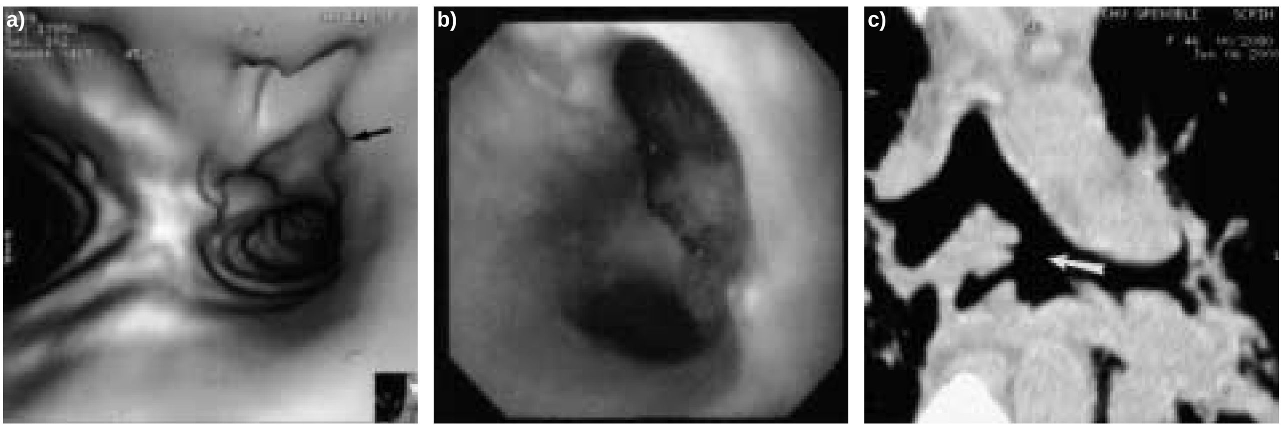

Fig. 2. – A 58-yr-old patient with tracheobronchial fistula. a) Virtual bronchoscopy view, the tip of the virtual endoscope being positioned in the end part of the trachea, shows the fistula (arrow). b) Real endoscopic view of the fistula. c) Sagittal multiplanar reformation shows the communication between the left main bronchus and the oesophagus (arrow).

target to biopsy are generated. FOB is then performed, the images being captured on a computer. Registration of the position relative to the tip of the real endoscope is obtained without an external device by image analysis of the bifurcations. As real and virtual images are similar, matching is performed in real time during the FOB procedure. Preliminary results showed promising localization accuracy of 1.1 mm.

VB has been proposed as a virtual tool for preparing various interventional bronchoscopic procedures, such as stent placement, laser photocoagulation, endobronchial cryotherapy, and endobronchial brachytherapy [24, 34]. To the best of the authors' knowledge, the real role of VB in these procedures has not been evaluated.

VB may be used as a complementary tool to axial CT images for the noninvasive follow-up of patients that had endobronchial procedures [9, 34].

The potential of virtual tools to provide images of the airways for synopsis should be emphasized at a time when multiple detector-row CT scanners may acquire the thorax in one apnoea with 1-mm sections, thereby generating up to 300 axial images [34].

Evaluation of physiological and pharmacological events in the lung may benefit from high-resolution HCT scanning and application of virtual tools, as it provides quantifiable information about regional responses of the bronchial tree and lung parenchyma to physiological and pharmacological stress [41].

In summary, axial CT images remain the basis for the review and interpretation of CT examinations of the airways. Owing to the number of 3D reconstructions that can be generated from HCT acquisitions, the time needed to create and review these images, and the clinical usefulness of each technique, radiologists usually use MPRs. Other virtual tools may highlight specific abnormalities and should be considered as complementary tools to axial CT images and MPRs. However, there may be rapid developments thanks to improvements in computer science.

Lung parenchyma and emphysema

Lung parenchyma

MIP and IPmin has been applied to high-resolution (1-mm section) focal volume acquisitions of lung parenchyma to either increase the perception and definition of infiltrative lung diseases (MIP) or to increase the perception of emphysema (IPmin) [14–16]. In a study including 26 patients suspected (n=6) or known (n=20) to have diffuse infiltrative lung disease, BHALLA *et al.* [14] showed that micronodules and peripheral pulmonary vessels were more obvious on MIP images than on conventional HRCT images. In a study including 81 patients with suspicion of pneumoconiosis (n=25), sarcoidosis (n=19), smoker bronchiolitis (n=17), and bronchiolitis of miscellaneous causes (n=20), RÉMY-JARDIN *et al.* [15] found three main advantages of MIP images over high-resolution (1-mm) and 8-mm CT images: 1) MIP images increased the sensitivity of CT examination in detecting micronodules as MIP images, using 5-mm sliding slabs, had a 100% sensitivity to detect micronodules *versus* 73% for HRCT images and 57% for 8-mm sections CT images; 2) MIP images allowed a more precise definition of the distribution of micronodules within the secondary pulmonary lobule, which is of particular importance in establishing the differential diagnosis of micronodular patterns; 3) in patients with inconclusive HR and 8-mm CT findings regarding the presence of micronodular opacities (17 of 81 patients), MIP images allowed for the detection of micronodular patterns that involved <25% of the lung surface. However, in patients with obvious micronodular pattern (46 of 81 patients) at conventional CT and in patients with normal HRCT (18 of 81 patients), MIP did not show any diagnostic superiority over HRCT. Therefore, MIP images are an additional tool used at second attention for adequate evaluation of mild forms of micronodular infiltration [8].

IPmin sliding thin slabs have the potential to select the voxels with the lowest density in the slab (fig. 3). This property has been used in a study including 29 patients without radiographical evidence of emphysema before surgery for lung cancer [16]. Pathological examination showed emphysema in 21 of 29 patients. IPmin images displayed a better sensitivity than

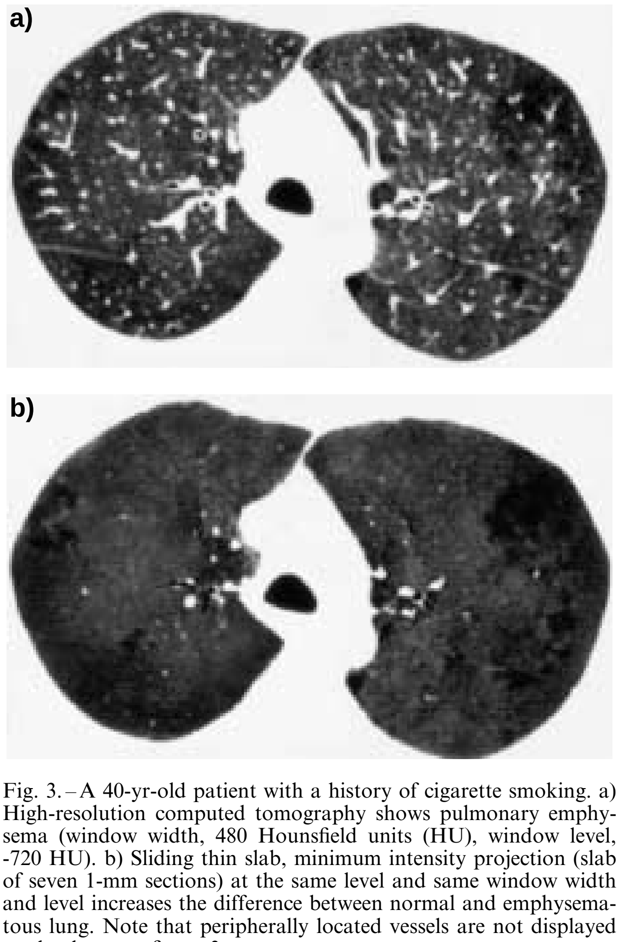

Fig. 3. – A 40-yr-old patient with a history of cigarette smoking. a) High-resolution computed tomography shows pulmonary emphysema (window width, 480 Hounsfield units (HU), window level, -720 HU). b) Sliding thin slab, minimum intensity projection (slab of seven 1-mm sections) at the same level and same window width and level increases the difference between normal and emphysematous lung. Note that peripherally located vessels are not displayed as clearly as on figure 3a.

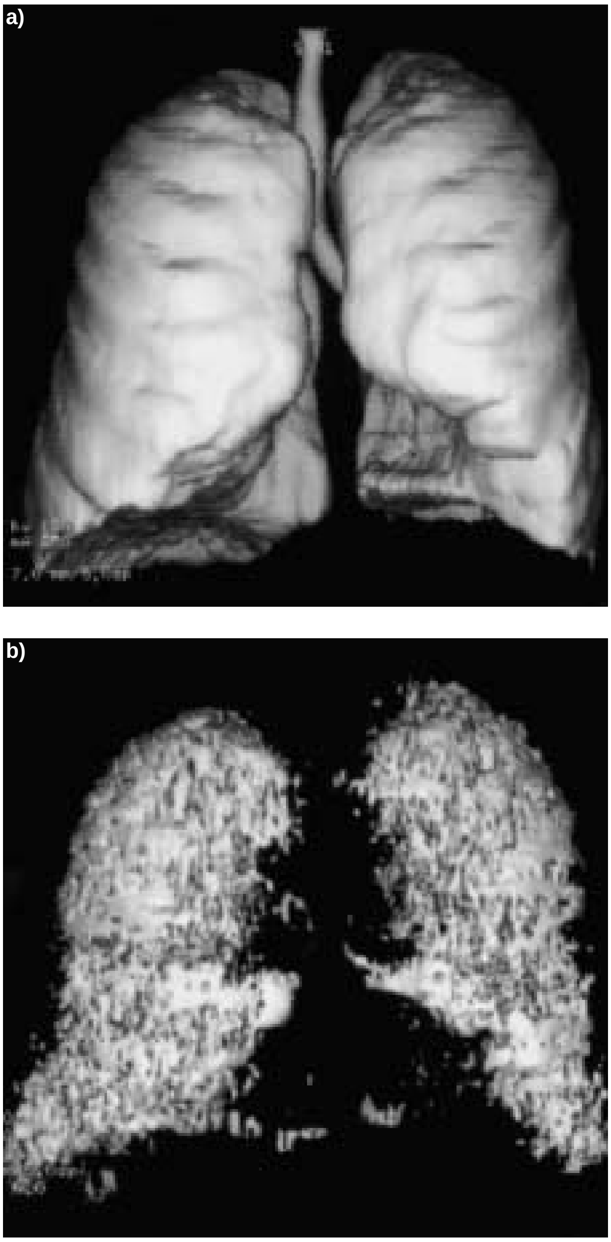

Fig. 4. – A 55-yr-old patient with a history of cigarette smoking and severe emphysema. Helical computed tomography before lung volume reduction surgery. HCT acquisition with 7-mm sections, reconstruction index of 3.5-mm. a) Three-dimensional surface shaded (3D SSD) model of the lungs using threshold values of (-1024, -400 Hounsfield units (HU)). b) 3D SSD model of the emphysematous lung using threshold values of (-1024, -950 HU shows heterogeneous distribution of emphysema.

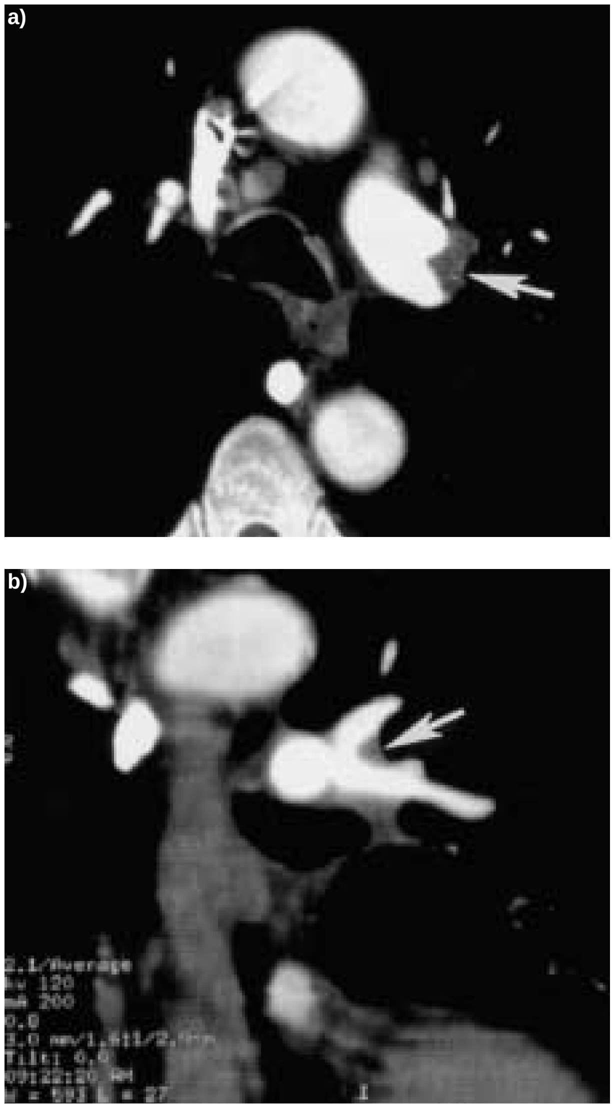

Fig. 5. – A 53-yr-old female with clinical suspicion of acute pulmonary embolism. Helical computed tomography angiography was performed with 3-mm sections. a) Axial computed tomography image at the level of the left pulmonary artery raises the suspicion of chronic pulmonary embolism (arrow). b) Coronal multiplanar reformation shows that low-density structure is due to externally located structure (arrow).

HRCT in detecting emphysema, with a sensitivity of 71% *versus* 54%. IPmin has the potential to enhance density changes related to small airway disease as compared to HRCT [42].

The sliding slab technique has the following limitations: 1) loss of information due to the selection of the lowest or highest value voxel along the slab requires the review of these virtual images along with the native 1-mm sections; 2) the need for a dedicated HCT acquisition which increases the radiation dose to the patient; and 3) great sensitivity to motion (cardiac, respiratory) which creates severe artefacts. This technique is, therefore, used at second attention in selected clinical cases in which it has been proved to be useful.

Quantification of pulmonary emphysema

HRCT quantification of emphysema is correlated with pulmonary function tests [43]. With the recent development of lung volume reduction surgery, attempts have been made to use 3D reconstructions of HCT data for quantifying emphysema and evaluating its distribution (fig. 4) [44–46]. In three series, the authors used 3D SSD models of the lungs and various threshold values to select pulmonary parenchyma and emphysema [44–46]. Their basic idea

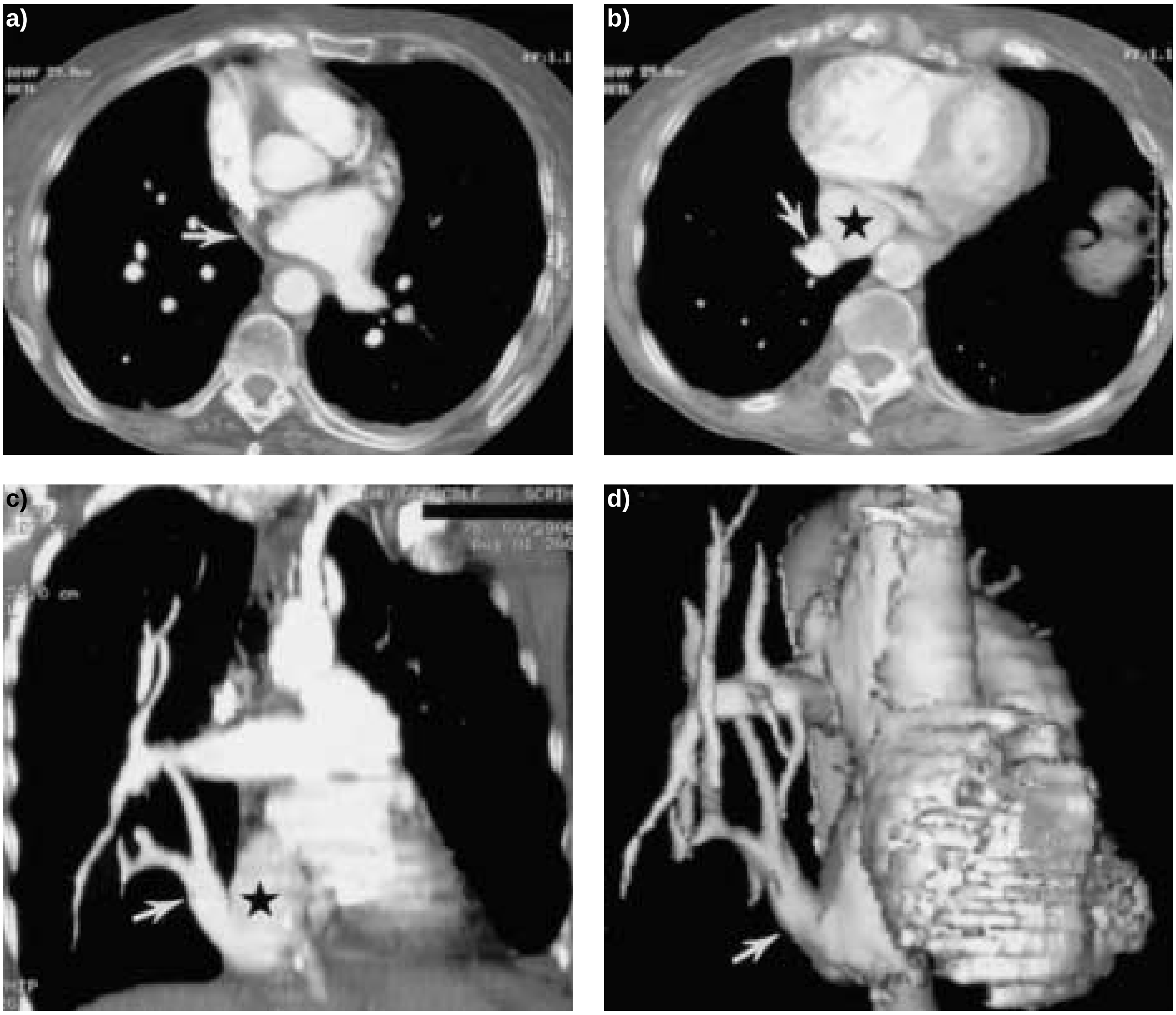

Fig. 6. – A 78-yr-old female with history of chronic dyspnoea and scimitar syndrome. Contrast enhanced computed tomography (CT) was acquired with 3-mm sections. a) Axial CT image at the level of the left atrium shows absence of left upper pulmonary vein (arrow). b) Axial CT image at the level of the right inferior pulmonary vein (arrow) shows enlargement of the vein that enters the right atrium (star). c) Coronal multiplanar reformation shows the enlargement and abnormal position of the right pulmonary vein (arrow) and the continuity with the right atrium (star). d) Three-dimensional surface shaded display view in a coronal projection of the malformation (arrow).

was that an abnormal emphysematous lung shows lower attenuation than a healthy lung. All authors concluded that 3D reconstructions correlated well with pulmonary function tests and provided accurate quantification and distribution of pulmonary emphysema. These considerations are of great value in improving the prediction of the postoperative functional outcome of patients. 3D SSD has been used in order to evaluate changes in lung volumes after lung volume reduction surgery [47]. HOLBERT *et al.* [47] showed that the volume of the surgically reduced lung decreased 22% and that the volume of the healthy lung increased 4%.

One series including 70 patients with severe emphysema (intermediately heterogeneous: 18; markedly heterogeneous: 42; homogeneous: 10), showed that functional improvement after lung volume reduction surgery was more closely correlated with the degree of emphysema heterogeneity showed by CT than with the degree of perfusion heterogeneity assessed by perfusion lung scintigraphy [48].

Pulmonary vessels

Computed tomography angiography (CTA) has dramatically changed the diagnostic approach to diseases of thoracic vessels [4] and has replaced conventional angiography in diagnostic algorithms. Although axial CT images remain the initial display mode, virtual tools have been used in selected indications.

In acute pulmonary embolism (PE), assessment of the pulmonary artery is performed by axial CT images. MPRs have been proposed in two major indications: to reconstruct obliquely-oriented arteries along their longitudinal axis in order to suppress partial volume effects that are responsible for false-positive

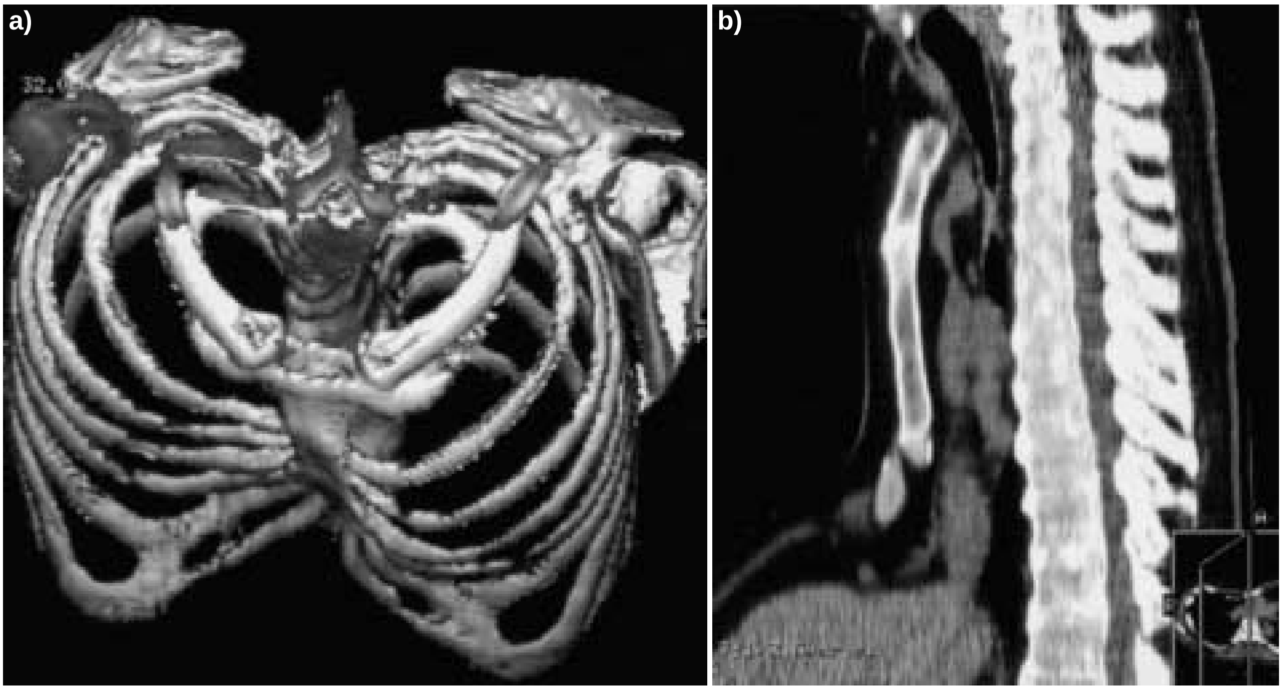

Fig. 7. – A 33-yr-old patient with pectus excavatum. a) Sagittal multiplanar reformation shows the compression of the mediastinum by the sternum. b) Three-dimensional surface shaded display of the thoracic wall gives an overview of the malformation.

diagnosis of PE in arteries [49]; to discriminate between peripherally located thrombi and externally located structures (fig. 5). Experience with virtual angioscopy is limited to one clinical report [21]. The other virtual tools have no indication in imaging acute PE.

HCT has been shown to be more accurate than MRI and conventional angiography in the diagnosis of chronic pulmonary thromboembolism of the central pulmonary artery [50]. In patients with such a condition, coronal and sagittal MPRs are complementary images to axial CT views in the disclosure of centrally located chronic thrombi and the definition of surgical approach [13].

External 3D imaging using surface or VR as well as STS MIP reconstructions, have been used to display pulmonary arteriovenous malformations (PAVM) [51, 52]. These virtual tools offer a noninvasive diagnostic approach in patients with hereditary haemorrhagic telangiectasia, a pretherapeutic map to guide interventional angiography and a noninvasive technique for follow-up after embolization [51]. Therefore, conventional angiography is currently dedicated to the embolization of PAVM that were previously investigated using HCT.

The same virtual techniques are useful in identifying and characterizing pulmonary vein abnormalities (fig. 6) [52, 53].

In patients with superior vena cava syndrome, CTA with MPRs and MIP highlight the cause of venous obstruction and allow preparation of endovascular stent placement by providing precise measurements [54]. CTA has replaced conventional phlebography for the diagnosis of superior vena cava syndrome.

Detection of arterial stenosis due to thoracic outlet syndrome, is eased by VR [55] as compared to axial CT images and MPR. HCTA and virtual tools may replace catheter angiography in this indication.

Pulmonary nodules

Low-dose HCT has recently been proposed as a technique for screening patients with a high risk of developing lung cancer [56]. Assessing the growth rate or more precisely the doubling-time of pulmonary nodules, is one of the best predictors of tumour malignancy. Volumetric growth estimation based on repeated 3D volumetric measurements of small pulmonary nodules was more accurate than estimation of growth rate on axial CT images [57]. 3D analysis of small pulmonary nodules may be one of the key tools for noninvasive assessment of the growth rate and morphology of small pulmonary nodules [58].

Diaphragm

HCT has enhanced the capabilities of CT in imaging the diaphragm [59]. Sagittal and coronal reformations are of particular importance in the evaluation of the peridiaphragmatic area [59]. A recent report underlines the role of HCT with MPR in sagittal and coronal planes in the diagnosis of diaphragmatic rupture after blunt trauma [60]. HCT with 3D reconstructions has been used to evaluate the effect of chronic hyperinflation on diaphragm length and surface area [61]. It has also been used after single-lung transplantation [62].

Chest wall

The natural high contrast of bony structures allows for the creation of spectacular 3D SSD or VR images of the thoracic wall (fig. 7). HCT scans were acquired in eight children who had corrective surgery for pectus excavatum and developed constricted thorax resulting from disturbed chest wall growth [63]. VR images were useful in preoperatively and postoperatively defining the orientation of the ribs and costal cartilages and their relationship to the sternum. Lung volumes were estimated before and after surgery with the same acquisition.

The respective roles of CT and magnetic resonance imaging (MRI) for the structural analysis of the chest wall remain controversial. Although MPR, 3D SSD, and VR have increased the value of CT in assessing the chest wall, MRI has superior contrast resolution, offers multiplanar imaging capabilities and high-resolution images by using surface coils. Therefore, MRI provides better results than CT in evaluating chest wall involvement in lung cancer [64], including the evaluation of superior sulcus tumour [65].

Conclusion

HCT has become a major technique for noninvasive assessment of the thorax. In clinical practice, it has nearly replaced more invasive radiological procedures such as pulmonary angiography and bronchography. Although axial CT images continue to be the basis for the review of the HCT acquisitions, 3D images enhance axial CT information in many clinical problems. Virtual tools may expand the clinical use of HCT by minimizing the requirement for invasive procedures such as bronchoscopy.

In the future, the use of virtual tools will certainly increase. Multiple detector-row computed tomography acquisition will provide isotropic (cubic) voxels, thereby increasing the quality of all types of three-dimensional visualization [66]. However, the total amount of generated axial computed tomography images will increase dramatically, creating difficulties in reviewing, interpreting, archiving, and filming computed tomography images. At the same time, increases in computer speed and power will allow for the performance of virtual simulations in real time. Three-dimensional and virtual images may become an alternative format for reviewing computed tomography acquisitions for interpretation [5]. However, the value of these images has to be assessed in comparison with axial computed tomography and anatomical images.

References

1. Kalender WA, Seissler W, Klotz E, Vock P. Spiral volumetric CT with single-breath-hold technique, continuous transport, and continuous scanner rotation. *Radiology* 1990; 176: 181–183.
2. Naidich DP. Helical computed tomography of the thorax. *Rad Clin North Am* 1994; 32: 759–774.
3. Touliopoulos P, Costello P. Helical (spiral) CT of the thorax. *Rad Clin North Am* 1995; 33: 843–861.
4. Rémy-Jardin M, Rémy J. Spiral CT angiography of the pulmonary circulation. *Radiology* 1999; 212: 615–636.
5. Fishman EK, Magid D, Ney DR, *et al.* Three-dimensional imaging. *Radiology* 1991; 181: 321–337.
6. Rubin GD, Beaulieu CF, Argiro V, *et al.* Perspective volume rendering of CT and MR images: applications for endoscopic imaging. *Radiology* 1996; 199: 321–330.
7. Richenberg JL, Hansell DM. Image processing and spiral CT of the thorax. *Br J Radiol* 1998; 71: 708–716.
8. Rémy J, Rémy-Jardin M, Artaud D, Fribourg M. Multiplanar and three-dimensional reconstruction techniques in CT: impact on chest diseases. *Eur Radiol* 1998; 8: 335–351.
9. Kauczor HU, Wolcke B, Fischer B, Mildenberg P, Lorenz J, Thelen M. Three-dimensional helical CT of the tracheobronchial tree: evaluation of imaging protocols and assessment of suspected stenoses with bronchoscopic correlation. *AJR* 1996; 167: 429–432.
10. Hooper KD, Iyriboz TA, Mahraj RPM, *et al.* CT bronchoscopy: optimization of imaging parameters. *Radiology* 1998; 209: 872–877.
11. Klingenbeck-Regn K, Schaller S, Flohr T, Ohnesorge B, Kopp AF, Baum U. Subsecond multi-slice computed tomography: basics and applications. *Eur J Radiol* 1999; 31: 110–124.
12. Napel S, Rubin GD, Jeffrey RB Jr. STS-MIP: a new reconstruction technique for CT of the chest. *J Comput Assist Tomogr* 1993; 17: 832–838.
13. Zeman RK, Silverman PM, Vieco PT, Costello P. CT angiography. *AJR* 1995; 165: 1079–1088.
14. Bhalla M, Naidich DP, McGuiness G, Gruden JF, Leitman BS, McCauley DI. Diffuse lung disease: assessment with helical CT-preliminary observations of the role of maximum and minimum intensity projection images. *Radiology* 1996; 200: 341–347.
15. Rémy-Jardin M, Rémy J, Artaud D, Deschildre F, Duhamel A. Diffuse infiltrative lung disease: clinical value of sliding-thin-slab maximum intensity projection CT scans in the detection of mild micronodular patterns. *Radiology* 1996; 200: 333–339.
16. Rémy-Jardin M, Rémy J, Gosselin B, Copin MC, Wurtz A, Duhamel A. Sliding thin slab, minimum intensity projection technique in the diagnosis of emphysema: histopathologic-CT correlation. *Radiology* 1996; 200: 665–671.
17. Kuszyk BS, Heath DG, Ney DR, *et al.* Fishman EK. CT angiography with volume rendering: imaging findings. *AJR* 1995; 165: 445–448.
18. Vining DJ, Liu K, Choplin RH, Haponik EF. Virtual bronchoscopy: relationships of virtual reality endobronchial simulations to actual bronchoscopic findings. *Chest* 1996; 109: 549–553.
19. Rémy-Jardin M, Rémy J, Artaud D, Fribourg M, Duhamel A. Volume rendering of the tracheobronchial tree: clinical evaluation of bronchographic images. *Radiology* 1998; 208: 761–770.
20. Ferretti GR, Vining DJ, Knoplioch J, Coulomb M. Tracheobronchial tree: three-dimensional spiral CT with bronchoscopic perspective. *J Comput Assist Tomogr* 1996; 20: 777–781.
21. Konen E, Rozenman J, Amitai M, Gayer G, Garniek A. Virtual CT angioscopy of pulmonary arteries in a patient with multiple pulmonary emboli. *AJR* 1998; 171: 399–400.

22. Summers RM. Navigational aids for real-time virtual bronchoscopy. *AJR* 1997; 168: 1165–1170.
23. Naidich DP, Gruden JF, McGuiness G, McCauley DI, Bhalla M. Volumetric (helical/spiral) CT (VCT) of the airways. *J Thorac Imaging* 1997; 12: 11–28.
24. Rémy J, Rémy-Jardin M, Bonnel F, Masson P. La tomodensitométrie spiralée (hélicoïdale) en pathologie trachéobronchique. *J Radiol* 2000; 81: 201–216.
25. Quint LE, Whyte RI, Kazerooni EA, *et al.* Stenosis of the central airways: evaluation by using helical CT with multiplanar reconstructions. *Radiology* 1995; 194: 871–877.
26. McAdams HP, Murray JG, Erasmus JJ, Goodman PC, Tapson VP, Davis RD. Telescoping bronchial anastomoses gor unilateral or bilateral sequential lung transplantation: CT appearance. *Radiology* 1997; 203: 202–206.
27. Rémy-Jardin M, Rémy J, Deschildre F, Artaud D, Ramon Ph, Edme JL. Obstructive lesions of the central airways: evaluation by using spiral CT with multiplanar and three-dimensional reformations. *Eur Radiol* 1996; 6: 807–816.
28. LoCicero J 3rd, Costello P, Campos CT, *et al.* Spiral CT with multiplanar and three-dimensional reconstructions accurately predicts tracheobronchial pathology. *Ann Thorac Surg* 1996; 62: 818–822.
29. Padhani AR, Fischman EK, Heitmiller RF, Wang KP, Wheeler JH, Kuhlman JE. Multiplanar display of spiral CT data of the pulmonary hilar in patients with lung cancer: preliminary observations. *Clin Imag* 1995; 19: 252–257.
30. Beigelman C, Howarth NR, Chartrand-Lefebre C, Grenier P. Congenital anomalies of tracheobronchial branching patterns: spiral CT aspects in adults. *Eur Radiol* 1998; 8: 79–85.
31. Lacrosse M, Trigaux JP, Van Beers BE, Weynants P. 3D spiral CT of the tracheobronchial tree. *J Comput Assist Tomogr* 1995; 19: 341–347.
32. Rodenwaldt, Kopka L, Roedel R, Margas A, Grabbe E. 3D virtual endoscopy of the upper airway: optimization of the scan parameters in a cadaver phantom and clinical assessment. *J Comput Assist Tomogr* 1997; 21: 405–411.
33. Ferretti G, Knoplioch J, Bricault I, Brambilla C, Coulomb M. Central airway stenoses: preliminary results of spiral-CT-generated virtual bronchoscopy simulations in 29 patients. *Eur Radiol* 1997; 7: 854–859.
34. Haponik EF, Aquino SL, Vining DJ. Virtual bronchoscopy. *Clin Chest Med* 1999; 20: 201–217.
35. Rapp-Bernhardt U, Welte T, Budinger M, Bernhardt TM. Comparison of three-dimensional virtual endoscopy with bronchoscopy in patients with oesophageal carcinoma infiltrating the tracheobronchial tree. *Br J Radiol* 1998; 71: 1271–1278.
36. Fleiter T, Merkle EM, Aschoff AJ, *et al.* Comparison of real-time virtual and fiberoptic bronchoscopy in patients with bronchial carcinoma: opportunities and limitations. *AJR* 1997; 169: 1591–1595.
37. Summers RM, Selbie WS, Malley JD, *et al.* Polypoid lesions of airways: early experience with computer-assisted detection by using virtual bronchoscopy and surface curvature. *Radiology* 1998; 208: 331–337.
38. Ferretti GR, Thony F, Bosson JL, Pison C, Arbib F, Coulomb M. Benign abnormalities and carcinoid tumors of the central airways: diagnostic impact of CT bronchography. *AJR* 2000; 174: 1307–1313.
39. McAdams HP, Goodman PC, Kussin P. Virtual bronchoscopy for directing transbronchial needle aspiration of hilar and mediastinal lymph nodes: a pilot study. *AJR* 1998; 170: 1361–1364.
40. Bricault I, Ferretti G, Cinquin P. Registration of real and CT-derived virtual bronchoscopic images to assist transbronchial biopsy. *IEEE Trans Med Imaging* 1998; 17: 703–714.
41. Kramer SS, Hoffman EA. Physiologic imaging of the lung with volumetric high-resolution CT. *J Thorac Imaging* 1995; 10: 280–290.
42. Fotheringham T, Chabat F, Hansell DM, *et al.* A comparison of methods for enhancing the detection of areas of decreased attenuation on CT caused by airways disease. *J Comput Assist Tomogr* 1999; 23: 385–389.
43. Kinsella M, Muller NL, Abboud RT, Morrison NJ, DyBuncio A. Quantitation of emphysema by computed tomography using a "density mask" program and correlation with pulmonary function tests. *Chest* 1990; 97: 315–321.
44. Park KJ, Bergin CJ, Clausen JL. Quantitation of emphysema with three-dimensional CT densitometry: comparison with two-dimensional analysis, visual emphysema scores, and pulmonary function test results. *Radiology* 1999; 211: 541–547.
45. Kauczor HU, Heussel CP, Fischer B, Klamm R, Mildenberger P, Thelen M. Assessment of lung volumes using helical CT at inspiration and expiration: comparison with pulmonary function tests. *AJR* 1998; 171: 1091–1095.
46. Mergo PJ, Williams WF, Gonzalez-Rothi R, *et al.* Three-dimensional volumetric assessment of abnormally low attenuation of the lung from routine helical CT: inspiratory and expiratory quantification. *AJR* 1998; 170: 1355–1360.
47. Holbert JM, Brown ML, Sciurba FC, Keenan RJ, Landreneau RJ, Holzer AD. Changes in lung volume and volume of emphysema after unilateral lung reduction surgery: analysis with CT lung densitometry. *Radiology* 1996; 201: 793–797.
48. Thurnheer R, Engel H, Weder W, *et al.* Role of lung perfusion scintigraphy in relation to chest computed tomography and pulmonary function in the evaluation of candidates for lung volume reduction surgery. *Am J Respir Crit Care Med* 1999; 159: 301–310.
49. Rémy-Jardin M, Rémy J, Cauvain O, Petyt L, Wannebroucq J, Beregi JP. Diagnosis of central pulmonary embolism with helical CT: role of two-dimensional multiplanar reformations. *AJR* 1995; 165: 1131–1138.
50. Bergin CJ, Sirlin CB, Hauschildt JP, *et al.* Chronic thromboembolism: diagnosis with helical CT and MR imaging with angiographic and surgical correlation. *Radiology* 1997; 204: 695–702.
51. Rémy J, Rémy-Jardin M, Giraud F, Wattinne L. Angioarchitecture of pulmonary arteriovenous malformations: clinical utility of three-dimensional helical CT. *Radiology* 1994; 191: 657–664.
52. Johnson PT, Heath DG, Kuszyk BS, Fishman EK. CT angiography: thoracic vascular imaging with interactive volume rendering technique. *J Comput Assist Tomogr* 1997; 21: 110–114.
53. Ferretti GR, Arbib F, Bertrand B, Coulomb M. Haemoptysis associated with pulmonary varices: demonstration using computed tomographic angiography. *Eur Respir J* 1998; 12: 989–992.
54. Thony F, Moro D, Witmeyer P, *et al.* Endovascular

treatment of superior vena cava obstruction in patients with malignancies. *Eur Radiol* 1999; 9: 965–971.

55. Rémy-Jardin M, Rémy J, Masson P, *et al.* CT angiography of thoracic outlet syndrome: evaluation of imaging protocols for the detection of arterial stenosis. *J Comput Assist Tomogr* 2000; 24: 349–361.
56. Henschke CI, McCauley DI, Yankelevitz DF, *et al.* Early Lung Cancer Action Project: overall design and findings from baseline screening. *Lancet* 1999; 354: 99–105.
57. Yankelevitz DF, Gupta R, Zhao B, Henschke CI. Small pulmonary nodules: evaluation with repeat CT-preliminary experience. *Radiology* 1999; 212: 561–566.
58. Reeves AP, Kostis WJ. Computer-aided diagnosis for lung cancer. *Radiol Clin North Am* 2000; 38: 497–509.
59. Brink JA, Heiken JP, Semenkovich J, Teefey SA, McClennan BL, Sagel SS. Abnormalities of the diaphragm and adjacent structures: findings on multiplanar spiral CT scans. *AJR* 1994; 163: 307–310.
60. Killeen KL, Mirvis SE, Shanmuganathan K. Helical CT of diaphragmatic rupture caused by blunt trauma. *AJR* 1999; 173: 1611–1616.
61. Cassart M, Pettiaux N, Gevenois PA, Paiva M, Estenne M. Effect of chronic hyperinflation on diaphragm length and surface area. *Am J Respir Crit Care Med* 1997; 156: 504–508.
62. Cassart M, Verbandt Y, de Francquen P, Gevenois PA, Estenne M. Diaphragm dimensions after single-lung transplantation for emphysema. *Am J Respir Crit Care Med* 1999; 159: 1992–1997.
63. Pretorius ES, Haller JA, Fishman EK. HCT with 3D reconstruction in children requiring reoperation for failure of chest wall growth after pectus excavatum surgery. Preliminary observations. *Clin Imaging* 1998; 22: 108–116.
64. Padovani B, Mouroux J, Seksik L, *et al.* Chest wall invasion by bronchogenic carcinoma: evaluation with MR imaging. *Radiology* 1993; 187: 33–38.
65. Hatabu H, Stock KW, Sher S, *et al.* Magnetic resonance imaging of the thorax. Past, present, and future. *Radiol North Am* 2000; 38: 593–620.
66. Levy RA. Three-dimensional craniocervical helical CT: is isotropic imaging possible? *Radiology* 1995; 197: 645–658.